

Introduction

Both carmustine and lomustine nitrosoureas decompose in the body to produce reactive intermediates that act as classic alkylating agents [1], therefore they cause strand breaks and cross-links in DNA. Additionally, they produce isocyanates, which inhibits DNA repair and the synthesis of RNA [2]. Carmustine is intravenously administered, while lomustine is prescribed orally. They are metabolized quickly and excreted gradually in the urine [3]. Since nitrosoureas are distinguished by their lipophilicity and ability to cross the boundary between blood and brain, so these properties are important in brain tumor [4], they are widely used in medicinal chemistry [5-7]. DNA-targeting anticancer drugs have been used in the clinic for over 60 years [8, 9]. Despite recent significant advances in cancer science, the process by which the most clinically important anticancer drugs destroy cells consists of replication interference, which can most easily be accomplished through alkylation with DNA [10].

Alkylating agents can be defined as compounds that are able to attach an alkyl group covalently to a biomolecule under physiological conditions (aqueous solution: 37 °C, pH: 7.4). In any phase of the cell cycle, DNA alkylating agents interact with resting and proliferating cells, however, they are more cytotoxic during the late G1 and S phases as there is not enough time to repair the damage before DNA synthesis. Covalent bonds can usually occur from attacks of either nucleophilic or electrophilic species to DNA, and in reality, certain nucleophiles (e.g., hydrazine, hydroxylamine, and bisulfite) have been known to attack DNA bases under physiological conditions. However, all of these bases nitrogen and oxygen atoms are nucleophiles, except for the nitrogen atoms that are involved in the nucleoside bond (N^9 or N^1 in purines or pyrimidines) [11]. Therapeutically useful drugs often behave as carbon electrophiles [10].

Two related but independent interactions regulate the attraction between nucleophiles and electrophiles, i.e., the electrostatic attraction between positive and negative charge (electrostatic control); and orbital overlap between the nucleophile HOMO and the electrophile LUMO (orbital control). These two forms of reactivity are respectively called "hard" and "soft". Consequently, the highly electronegative oxygen atoms react under electrostatic control and are considered to be "hard" nucleophiles, and hence, they react with "hard" electrophiles that are their cationic character. Nitrogen atoms in DNA bases are softer nucleophilic than oxygen atoms, therefore, many therapeutically useful alkylating agents are relatively "soft" electrophiles [12].

Density Functional Theory (DFT) is one of the theoretical methods used for simulating the synthesized compounds [13-

17]. The DFT method is a significant area of interest because it has a perfect analytical capacity for the structural, spectral, and electronic properties of many molecules and has a high agreement with the experimental data [15, 18-20]. B3LYP method is one of the DFT functions that showed an important precision in predicting the electronic, energetic, and spectral properties of various molecules; therefore, it's called the brain of quantum chemistry [21-24].

In the present work, each of the energy bandgaps, molecular geometry, frontier molecular orbitals, MEP, and Mulliken atomic charge are scrutinized using DFT/B3LYP method at 6-311++G(d, p) basis set for both molecules.

Computational Details

The whole series of quantum calculations are performed using the Gaussian 09W program package. Density Functional Theory (DFT) and Hartree-Fock (HF) methods with B3LYP levels were used through the 6-311++G(d, p) basis set [25, 26]. Firstly, the molecules have been optimized at various basis sets (3-21G, 6-31G, 6-31+G, 6-31++G, 6-311G, 6-311+G, 6-311++G), then the energy bandgaps at mentioned basis sets were determined and listed in Table 1. The B3LYP/6-311++G level was chosen for the entire calculations. The molecular geometry was also determined for the drugs. Table 2 presents the comparatively optimized structural parameters, such as bond length, bond angle, and dihedral angle.

The electronic properties, HOMO–LUMO energies, were computed to estimate the more reactive molecule [27-29]. Additionally, some important parameters, including ionization potential, electron affinity, electronegativity, the dipole moment properties, chemical hardness, and chemical softness were calculated; furthermore, molecular electrostatic potentials and Mulliken atomic charges have been also presented.

Result and Discussion

Energy Band Gaps

The first step of the theoretical work was to find the optimized molecular structure using the Gaussian 09 software [30, 31]. Table 1 lists the energy band gaps related to basis sets (3-21G, 6-31G, 6-31+G, 6-31++G, 6-311G, 6-311+G, 6-311++G). The energy bandgaps for the HF method have higher values compared to the DFT. The basis set of 6-311++G(d, p) has been chosen for DFT method because they give a minimum energy band gap compared to the other known methods and sets, therefore they are more reliable and provide better results.

Table 1. The energy band gaps of various basis set using HF and DFT methods for carmustine and lomustine molecules

| Basis sets | Carmustine | | Lomustine | |
|------------|---------------------------------------|--|---------------------------------------|--|
| | HF method Energy band gaps (eV) | DFT method Energy band gaps (eV) | HF method Energy band gaps (eV) | DFT method Energy band gaps (eV) |
| 3-21G | 13.51382 | 4.60284 | 12.64740 | 4.45481 |
| 6-31G | 13.42783 | 4.61889 | 12.66536 | 4.44936 |
| 6-31G+ | 13.13748 | 4.58760 | 12.39515 | 4.43576 |
| 6-31G++ | 12.40957 | 4.58569 | 11.79704 | 4.43077 |
| 6-311G | 13.41423 | 4.61944 | 12.64169 | 4.45154 |
| 6-311G+ | 13.03598 | 4.58787 | 12.36046 | 4.43657 |
| 6-311G++ | 12.38046 | 4.58542 | 11.77064 | 4.42977 |

Molecular Geometry

The optimized molecular structure of carmustine and lomustine is shown in Figures 1b and 2b, respectively. The atoms in both molecules have been labeled. The parameters for the geometry-optimized structures, including bond lengths, bond angles, and dihedral angles, for both molecules are listed in Table 2.

Fun et al. recorded the bond length of C-C as 1.500 Å [32]. For carmustine molecule, we found that the bond length of C₁₀-C₉ and C₃-C₂ are 1.518 and 1.524 Å, respectively, whereas for the lomustine compound, the C-C bond length in the cycle is between 1.540 Å -1.543 Å. Meanwhile, the bond length of C₁₆-C₁₇ out of the cycle was recorded as 1.514 Å for the lomustine molecule. Also, C=O is another bond that appears in both compounds' structure. This type of bond usually seems to have a bond length of 1.209 Å [33]. We found that the bond length of C₆=O₁₂ for carmustine is 1.243 Å, while the bond length of C₁₃=O₁₄ in lomustine is 1.246 Å. The actual bond length of C-N and C=N was recorded to be 1.468 Å and 1.380 Å, respectively [34]. From DFT calculations using B3LYP/6-311++G, the bond length for C-

N in the carmustine compound was estimated from 1.439 to 1.477 Å, and the bond length of C₆=N₇ was 1.354. In lomustine, the single bonded C-N has bond lengths between 1.472 and 1.483 Å; and the double bonded C=N has 1.345 Å.

Allen et al. obtained the bond length of C-Cl as 1.849 Å [35]. In the current study, the bond lengths of C₁₀-Cl₁₁ and C₂-Cl₁ are 1.890 and 1.887 Å, respectively for carmustine molecule; the length of the bond C₁₇-Cl₂₀ in lomustine is 1.892 Å. It has also reported that the bond lengths of N-N and N=O are 1.370 Å [35] and 1.210 Å [36], respectively. As indicated in Table 1, in carmustine the bond length between N₄ and N₅ is 1.363 Å, and in lomustine, the N₁₅-N₁₈ has bond length of 1.357 Å. The result revealed that N₅=O₈ bond length is 1.255 Å in carmustine compound meanwhile for lomustine, the length of N₁₈=O₁₉ bond is 1.267 Å.

Fig. 1 and Fig. 2. show the geometrical structure of both molecules. This is the reason why the bond angle and dihedral angle of carmustine and lomustine molecules are different. Table 2 displays the values for the calculated geometrical parameters.

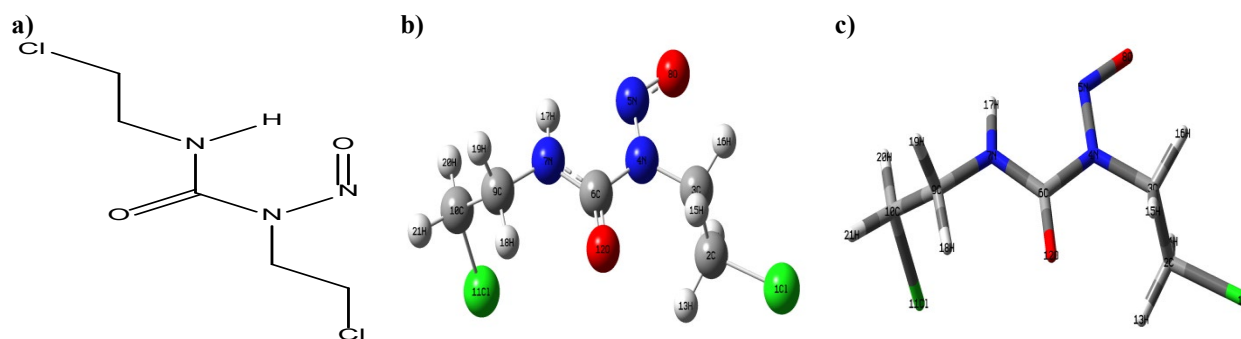


Fig. 1 (a) Molecular structure of carmustine molecule. (b) The theoretical geometric structure of the title compound (with B3LYP/6-311++G(d,p) level). (c) Molecule tube layer shape of optimized carmustine compound for the B3LYP/6-311++G(d,p) level

a)

b)

c)

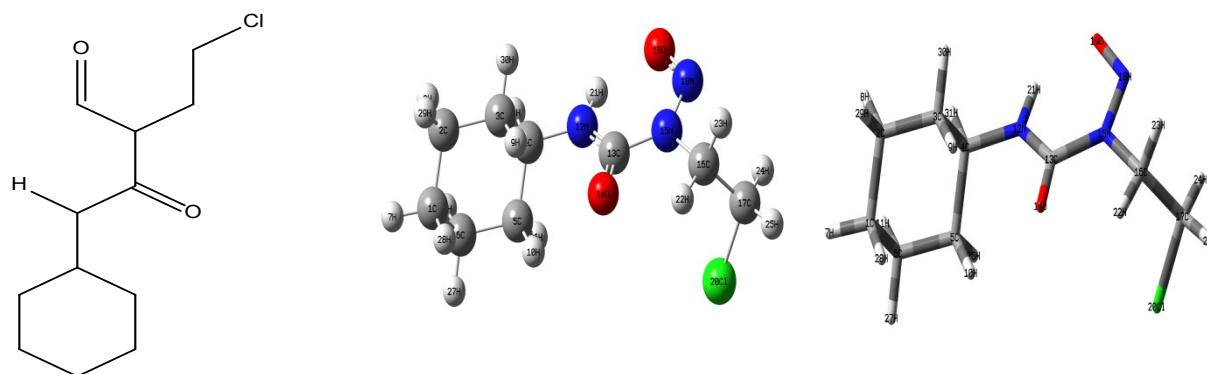


Fig. 2. (a) Molecular structure of lomustine molecule. (b) The theoretical geometric structure of the title compound (with B3LYP/6-311++G(d,p) level). (c) Molecule tube layer shape of optimized lomustine compound for the B3LYP/6-311++G(d,p) level

Frontier Molecular Orbitals

The concept of the molecular orbital characteristic is the relationship between highest occupied molecular (HOMO) orbital and unoccupied molecular orbital (LUMO) with HOMO-1 and LUMO+1 [37, 38]. The frontier molecular orbital theory plays an essential role in quantum chemistry [20]. It can be used for clarifying the interactions, i.e., it helps to identify molecular attributes that is associated with the discrepancy between the HOMO and LUMO [39]. The LUMO energy is related to electrons affinity and identifies the sensitivity of a molecule to a nucleophilic attack. On the other hand, the HOMO energy is related to the ionization

potential and determines the sensitivity of a molecule to an electrophilic attack [40]. The chemical activity of the compound is commonly argued by the energy differences between HOMO and LUMO, and the potential differences between them. The energy bandgap significantly related to the reactivity of a molecule. Fig. 3 illustrates the configuration and energy levels of carmustine and lomustine orbitals, including HOMO-1, HOMO, LUMO, and LUMO+1, which were determined by B3LYP/6-311++G. The result shows that carmustine has a higher energy level between HOMO and LUMO compared to lomustine, which means lomustine is more reactive than carmustine due to the lower energy levels.

Table 2: The parameters of molecular structure for carmustine and lomustine by the B3LYP/6-311++G(d,p) basis set

| Carmustine | | Lomustine | |
|----------------------|---------------------|-------------------------|---------------------|
| Atoms | Bond Length (Å) | Atoms | Bond Length (Å) |
| Cl(1)-C(2) | 1.887827 | C(2)-C(1) | 1.540332 |
| C(2)-C(3) | 1.524625 | C(3)-C(2) | 1.541426 |
| C(3)-N(4) | 1.477168 | C(4)-C(3) | 1.543191 |
| N(4)-N(5) | 1.363894 | C(5)-C(4) | 1.542819 |
| N(4)-C(6) | 1.439865 | C(6)-C(4) | 1.542104 |
| C(6)-N(7) | 1.354818 | C(6)-C(1) | 1.540375 |
| N(5)-O(8) | 1.255318 | N(12)-C(4) | 1.483569 |
| N(7)-C(9) | 1.459565 | C(13)-N(12) | 1.34592 |
| C(9)-C(10) | 1.518015 | O(14)-C(13) | 1.246335 |
| C(10)-Cl(11) | 1.890142 | N(15)-C(13) | 1.47282 |
| C(6)-O(12) | 1.24353 | C(16)-N(15) | 1.480265 |
| | | C(17)-C(16) | 1.514624 |
| | | N(18)-N(15) | 1.357429 |
| | | O(19)-N(18) | 1.26748 |
| | | Cl(20)-C(17) | 1.892018 |
| Atoms | Bond Angles (°) | Atoms | Bond Angles (°) |
| Cl(1)-C(2)-C(3) | 108.5331 | C(1)-C(2)-C(3) | 111.618 |
| C(2)-C(3)-N(4) | 110.8548 | C(2)-C(3)-C(4) | 110.7686 |
| C(3)-N(4)-N(5) | 122.75 | C(3)-C(4)-C(5) | 111.7081 |
| C(3)-N(4)-C(6) | 120.0493 | C(2)-C(1)-C(6) | 111.2473 |
| N(4)-C(6)-N(7) | 115.1585 | C(3)-C(4)-N(12) | 112.3668 |
| N(4)-N(5)-O(8) | 115.7134 | C(4)-N(12)-C(13) | 123.8034 |
| C(6)-N(7)-C(9) | 121.7497 | N(12)-C(13)-O(14) | 126.3774 |
| N(7)-C(9)-C(10) | 113.1098 | N(12)-C(13)-N(15) | 116.0426 |
| C(9)-C(10)-Cl(11) | 111.4735 | C(13)-N(15)-C(16) | 117.4792 |
| N(4)-C(6)-O(12) | 119.0179 | N(15)-C(16)-C(17) | 112.9517 |
| | | C(13)-N(15)-N(18) | 129.7387 |
| | | N(15)-N(18)-O(19) | 117.9452 |
| | | C(16)-C(17)-Cl(20) | 111.4534 |
| Atoms | Dihedral Angles (°) | Atoms | Dihedral Angles (°) |
| Cl(1)-C(2)-C(3)-N(4) | 178.9694 | N(12)-C(13)-N(15)-C(16) | -174.407 |
| C(3)-N(4)-C(6)-N(7) | 115.1584 | C(13)-N(15)-C(16)-C(17) | 120.2897 |
| N(4)-C(6)-N(7)-C(9) | 176.516 | | |
| C(6)-N(7)-C(9)-C(10) | 113.1097 | | |

Moreover, some molecular parameters can be determined according to HOMO and LUMO. The minimum amount of energy needs to remove an electron from the atom or molecule in a gaseous state is known as the ionization potential (I), which is defined as:

$$I = -E_{HOMO} \quad (1)$$

While, the amount of energy is expelled from a molecule in gaseous state by capture an electron to the molecule; this process is called electron affinity (A):

$$A = -E_{LUMO} \quad (2)$$

Additionally, electronegativity (X) represents an atom's ability to attract electrons. Chemical hardness (η) is a form of weight transfer prevention in molecules. In another word, the higher the chemical hardness values of the molecules the lower or unchanged the weight transfer [41, 42]. Also, the chemical softness inversely related to the molecular hardness [43-46]. The electronegativity, molecular hardness and softness, respectively, can be found as:

$$X = \frac{I+A}{2} \quad (3)$$

$$\eta = \frac{I-A}{2} \quad (4)$$

$$S = \frac{1}{2\eta} \quad (5)$$

Table 3 lists the parameter values of the electronic structure obtained by the B3LYP method. The results demonstrate that the lomustine has lower hardness and softer compared to the carmustine.

Dipole moment happens when charging is split, e.g., it occurs between two ions in an ionic bond, or between atoms in a covalent bond. Dipole moments arise from the electronegativity differences. Further differences in electronegativity increase the dipole moment [47]. The total dipole moment of carmustine is 5.415 (C.m), which is higher than in lomustine with dipole moment value of 1.667 (C.m). This result indicates that carmustine has greater electron negativity than lomustine. The axial dipole moments for title compounds are listed in Table 3.

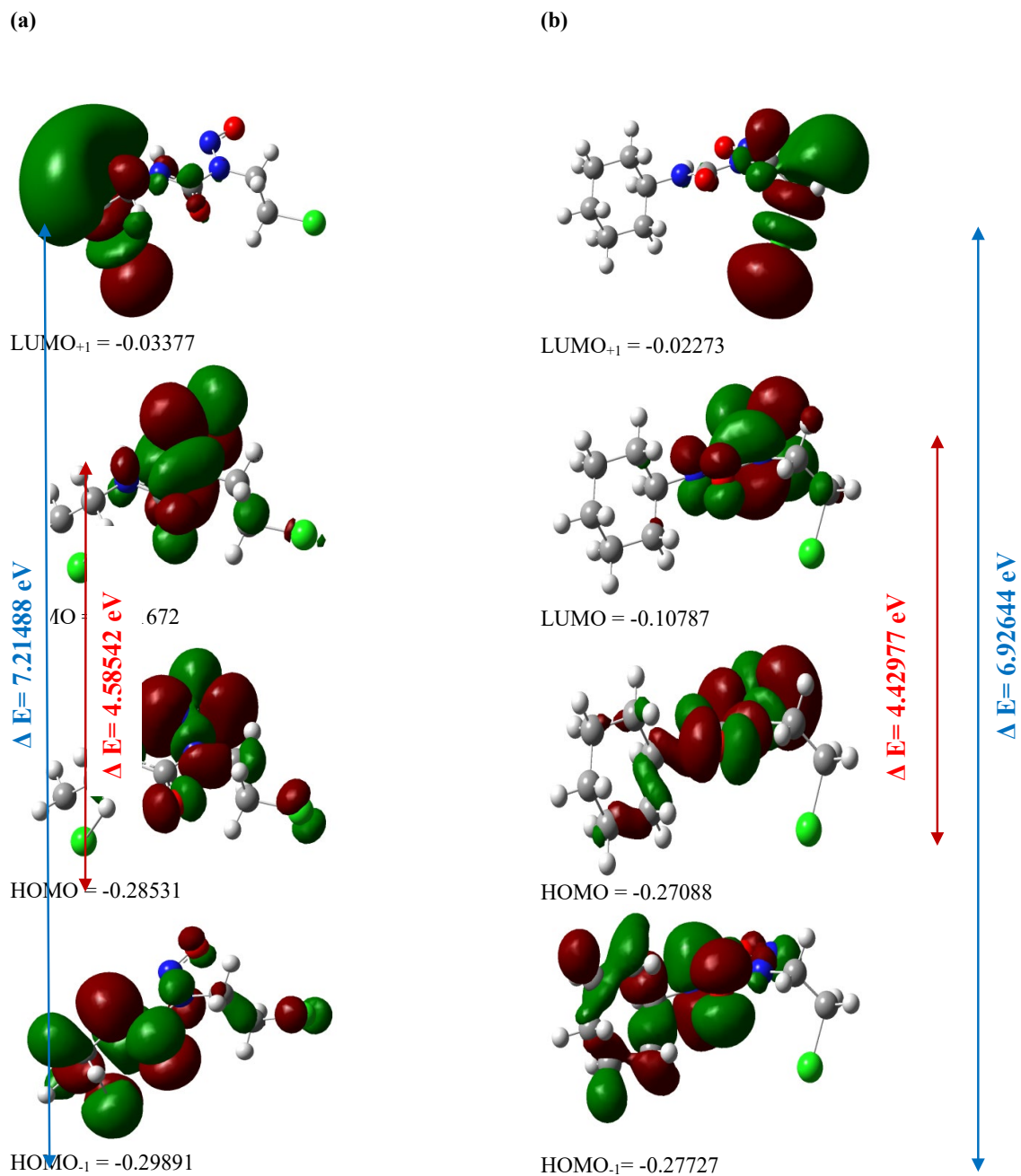


Fig. 3 Molecular orbital surfaces and energy levels for the HOMO, HOMO₋₁, LUMO and LUMO₊₁ analysis by B3LYP/6-311++G; a) Carmustine; b) Lomustine

Table 3. Electronic parameters for title molecules (carmustine & lomustine)

| At B3LYP/6-311++G basis set | Equations | Result of Carmustine | Result of Lomustine |
|---|--|----------------------|---------------------|
| E_{LUMO+1} (eV) | E_{LUMO+1} | -0.03377 | -0.02273 |
| E_{LUMO} (eV) | E_{LUMO} | -0.11672 | -0.10787 |
| E_{HOMO} (eV) | E_{HOMO} | -0.28531 | -0.27088 |
| E_{HOMO-1} (eV) | E_{HOMO-1} | -0.29891 | -0.27727 |
| $\Delta E = E_{HOMO} - E_{LUMO}$ (eV) | $HOMO - LUMO \times 27.2116$ | 4.58542 | 4.42977 |
| $\Delta E = E_{HOMO-1} - E_{LUMO+1}$ (eV) | $HOMO_{-1} - LUMO_{+1} \times 27.2116$ | 7.21488 | 6.92644 |
| I (eV) | $I = -E_{HOMO}$ | 0.28531 | 0.27088 |
| A (eV) | $A = -E_{LUMO}$ | 0.11672 | 0.10787 |
| X (eV) | $X = I + A/2$ | 0.34367 | 0.32481 |
| η (eV) | $\eta = I - A/2$ | 0.22695 | 0.21694 |
| S (eV) | $S = I/2\eta$ | 2.20312 | 2.30478 |
| μ_{total} (C.m) | | 5.4155 | 1.6679 |
| μ_x (C.m) | | -4.6662 | -0.7254 |
| μ_y (C.m) | | 2.4007 | 0.9650 |
| μ_z (C.m) | | 1.3383 | 1.1508 |

Molecular Electrostatic Potential

Electrostatic potential maps display the charging distributions of molecules in 3D, which allow observation of charging differences in the various areas of a molecule. If the distributions of charges are known, the nature of the interaction between molecules can be clarified. In addition, the analysis and anticipation of a molecule's reactive behavior can be effectively carried out depending on the molecular electrostatic potential (ESP) map produced by the nuclei and electrons of the molecule, which are known as charging distributions, in the space surrounding the molecule [48-50]. Different colors represent different surface electrostatic potentials, with red and blue signify the most negative and positive potential, respectively. In accordance with the color spectrum, colors are assigned to intermediate potentials, such that red < orange < yellow < green < blue. The red areas on the map correspond to the molecular areas with the maximum electrons abundance; while the blue areas

correspond to the molecular areas with the lowest total electrons [51, 52]. The MEP map's color code ranged from -0.0659 a.u. (deepest red) to +0.0659 a.u. (deepest blue) for carmustine compounds, while the charge distribution for lomustine molecule is lower and appeared between -0.04649 a.u (deepest red) and +0.04649 a.u. (deepest blue). The Blue area and red area, respectively, represent the greatest attraction and greatest repulsion.

Fig. 4a and Fig. 4b illustrate the mapping of the carmustine potential electrostatic surface, and Fig. 5a and Fig. 5b represent the mapping of the lomustine potential electrostatic surface. The results show that the oxygen atoms exhibited the greatest repulsion. The compound negative areas were located primarily over the carbonyl (C = O) groups, as indicated in the MEP map, while the maximum positive regions were appeared over the CHNCl groups. The MEPs of both molecules are very similar. This result also gives information about which region is suitable to attach other molecules.

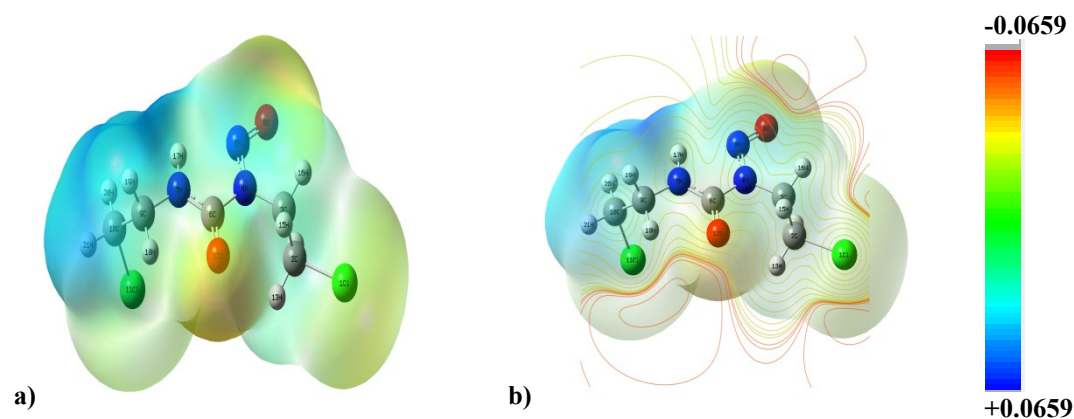


Fig. 4 a) Molecular electrostatic potential map calculated at B3LYP/6311++G(d,p) level for carmustine. (b) Contour shape of the title compound.

Mulliken Atomic Charge

Mulliken atomic charge calculation plays an important role in applying quantum chemical calculation to the molecular system because it can be utilized for obtaining the atomic charges effect dipole moment, molecular polarizabilities, electronic structure, and many other properties of molecular systems. The distribution of charges over the atoms suggests the formation of donor and acceptor pairs that involve the transfer of charges within the molecule [19, 53]. The carmustine molecular structure consists of twenty-one atoms: five-carbon, nine hydrogens, two chlorides, three nitrogens, and two oxygen atoms. Whereas the molecular composition of lomustine is composed of thirty-one atoms: nine carbons, sixteen hydrogens, one chloride, three

nitrogens, and two oxygen atoms. Table 4 illustrates the Mulliken net charges determined by Gaussian 09 in the gas phase by using the DFT method with the 6-311++G(d, p) basis set for title compounds. The representation of the plotted atomic charges is revealed in Fig. 5 The results indicated that H₁₇ has the highest positive atomic charge (0.48041 C) and N₄ has the lowest positive charge (0.038007 C) in the carmustine compound. Meanwhile, the maximum positive charge occurred in lomustine at H₂₁ (0.495916 C) and the minimum positive charge at N₁₂ was 0.038026 C. In addition, C₁₀ has the largest negative atomic charge (-1.020167 C) and O₈ has the smallest value atomic charge (-0.061736 C) in the carmustine. The maximum negative charge is -1.211594 C due to C₁₇ and the minimum value is -0.077639 C seemed to O₁₉ in the lomustine molecule.

Table 4. Atomic charge distribution for carmustine and lomustine molecules

| Carmustine | | Lomustine | |
|------------|-------------|-----------|-------------|
| Atoms | Charges (C) | Atoms | Charges (C) |
| Cl(1) | 0.245705 | C(1) | -0.571865 |
| C(2) | -0.723745 | C(2) | -0.67436 |
| C(3) | -0.632933 | C(3) | -0.1537 |
| N(4) | 0.038007 | C(4) | -0.523925 |
| N(5) | -0.084659 | C(5) | -0.186298 |
| C(6) | 0.038136 | C(6) | -0.71686 |
| N(7) | -0.218882 | H(7) | 0.268355 |
| O(8) | -0.061736 | H(8) | 0.241933 |
| C(9) | -0.272086 | H(9) | 0.318815 |
| C(10) | -1.020167 | H(10) | 0.316402 |
| Cl(11) | 0.228256 | H(11) | 0.24314 |
| O(12) | -0.338915 | N(12) | 0.038026 |
| H(13) | 0.310963 | C(13) | -0.208497 |

| | | | |
|-------|----------|--------|-----------|
| H(14) | 0.27553 | O(14) | -0.289864 |
| H(15) | 0.285225 | N(15) | 0.214589 |
| H(16) | 0.292455 | C(16) | -0.318746 |
| H(17) | 0.48041 | C(17) | -1.211594 |
| H(18) | 0.324231 | N(18) | -0.236056 |
| H(19) | 0.255278 | O(19) | -0.077639 |
| H(20) | 0.291757 | Cl(20) | 0.226689 |
| H(21) | 0.28717 | H(21) | 0.495916 |
| | | H(22) | 0.325239 |
| | | H(23) | 0.293949 |
| | | H(24) | 0.338903 |
| | | H(25) | 0.301134 |
| | | H(26) | 0.258118 |
| | | H(27) | 0.271717 |
| | | H(28) | 0.23759 |
| | | H(29) | 0.270122 |
| | | H(30) | 0.255325 |
| | | H(31) | 0.253442 |

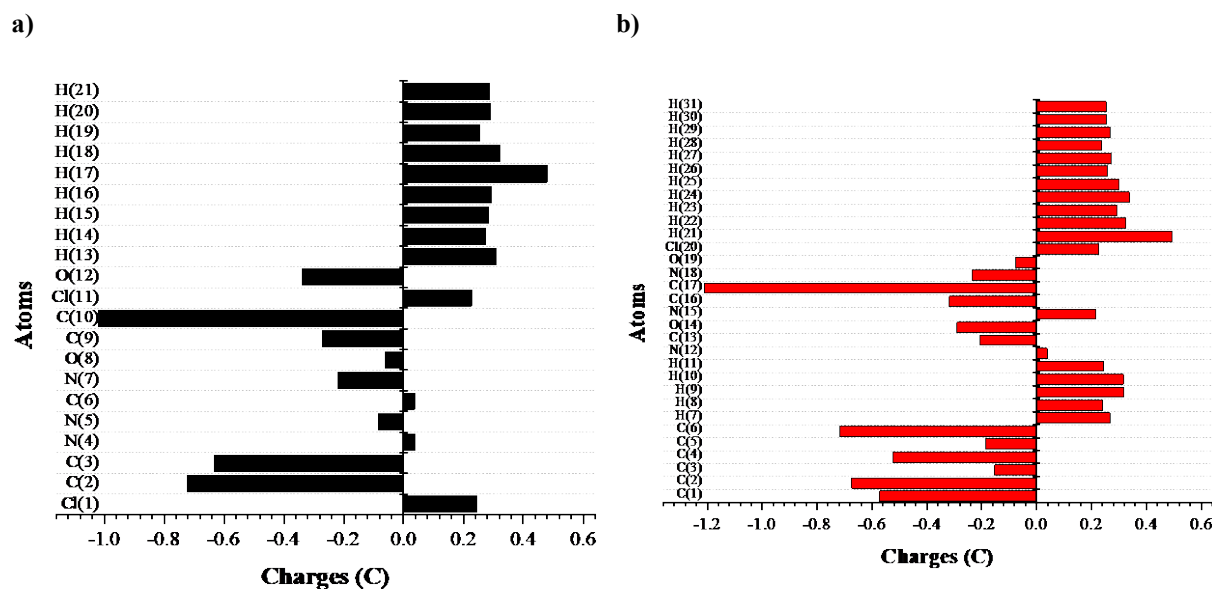


Fig. 5. The Mulliken atomic charge plot at B3LYP/6-311++G level; a) Carmustine; b) Lomustine

Conclusion

The molecular geometry was optimized to determine the energy bandgaps using Gaussian 09 software. The energy bandgaps for the HF method were higher than the DFT. The 6-311++G(d, p) basis set was chosen for the DFT method because the results are more accurate. The parameters, including bond length, bond angle, and dihedral angle were calculated for both molecules. The resulting illustration culminated in a clear agreement with previous literature. Both molecules have a various geometrical structure, so the

bond angle and dihedral angle of the molecules were different. The energy bandgaps between HOMO-1, HOMO, LUMO, and LUMO+1 have been determined to indicate the molecule's reactivity and the structure properties. Carmustine molecule has higher energy levels. Lomustine is less hard and softer than carmustine, thus, lomustine is more reactive than carmustine due to lower energy levels and more softness. The electrostatic potential of both title compounds shows that negative regions are correlated with carbonyl groups and that maximum positive regions are identified in the CHNCl groups. The distribution of Mulliken charges was

examined to look at the higher areas of electron density as possible interaction sites, such as oxygen.

Conflict of interest There is no conflict of interest of this manuscript, according to the authors.

References

- [1] Dowd F. J., Johnson B. and Mariotti A., *Pharmacology and Therapeutics for Dentistry-E-Book*. 2016.
- [2] Ozols R. F., *Molecular and clinical advances in anticancer drug resistance*. 2012.
- [3] Weber G. F., *Molecular therapies of cancer*. 2015.
- [4] Laquintana V., Trapani A., Denora N., Wang F., Gallo J. M. and Trapani G., "New strategies to deliver anticancer drugs to brain tumors", *Expert opinion on drug delivery*, 2009, 6(10): 1017-1032.
- [5] Syrkin A. and Gorbacheva L., "The biochemical mechanisms of the action of N-alkyl-N-nitrosoureas. The possible reasons for drug resistance to these compounds", *Eksperimental'naiia i klinicheskaia farmakologiya*, 1996, 59(2): 69.
- [6] Nabors L. B., Surboeck B. and Grisold W., *Complications from pharmacotherapy*. 235-250 *Handbook of Clinical Neurology*. Elsevier; (2016).
- [7] Dulohery M. M., Maldonado F. and Limper A. H., *Drug-Induced Pulmonary Disease*. 1275-1294. e17 *Murray and Nadel's Textbook of Respiratory Medicine*. Elsevier; (2016).
- [8] Hurley L. H., "DNA and its associated processes as targets for cancer therapy", *Nature Reviews Cancer*, 2002, 2(3): 188-200.
- [9] Ali A. and Bhattacharya S., "DNA binders in clinical trials and chemotherapy", *Bioorganic & medicinal chemistry*, 2014, 22(16): 4506-4521.
- [10] Nelson S. M., Ferguson L. R. and Denny W. A., "DNA and the chromosome-varied targets for chemotherapy", *Cell & chromosome*, 2004, 3(1): 2.
- [11] Demir S., Pekdemir S., Keser S., Karatepe A., KOPARIR M. and Karatepe M., "Antioxidant and antiproliferative properties of some 2-(4h-[1, 2, 4] Triazol-3-Yl-sulfanyl)-acetamide derivatives", *International Journal of Pure and Applied Sciences*, 2021, 7(3): 472-479.
- [12] Blackburn G. M., Gait M. J., Loakes D., Williams D. M., Egli M., Flavell A., Allen S., Fisher J., Haq S. I. and Pyle A. M., *Nucleic acids in chemistry and biology*. 2006.
- [13] Ahmed L., OMER R. and Kebiroglu H., "A theoretical study on Dopamine molecule", *Journal of Physical Chemistry and Functional Materials*, 2019, 2(2): 66-72.
- [14] OMER L. A. and Rebaz O., "Computational Study on Paracetamol Drug", *Journal of Physical Chemistry and Functional Materials*, 2020, 3(1): 9-13.
- [15] Neese F., "Prediction of molecular properties and molecular spectroscopy with density functional theory: From fundamental theory to exchange-coupling", *Coordination Chemistry Reviews*, 2009, 253(5-6): 526-563.
- [16] Qader I. N., Mohammad A., Azeez Y. H., Agid R. S., Hassan H. S. and Al-Nabawi S. H. M., "Chemical Structural and Vibrational Analysis of Potassium Acetate: A Density Function Theory Study", *Journal of Physical Chemistry and Functional Materials*, 2(1): 22-24.
- [17] AHMED L. and Rebaz O., "The Role of the Various Solvent Polarities on Piperine Reactivity and Stability", *Journal of Physical Chemistry and Functional Materials*, 4(2): 10-16.
- [18] Koparir P., Sarac K., Orek C. and Koparir M., "Molecular structure, spectroscopic properties and quantum chemical calculations of 8-t-butyl-4-methyl-2H-chromen-2-one", *Journal of Molecular Structure*, 2016, 1123: 407-415.
- [19] Koparir M., Orek C., Koparir P. and Sarac K., "Synthesis, experimental, theoretical characterization and biological activities of 4-ethyl-5-(2-hydroxyphenyl)-2H-1, 2, 4-triazole-3 (4H)-thione", *Spectrochimica Acta Part A: Molecular and Biomolecular Spectroscopy*, 2013, 105: 522-531.
- [20] Celikezen F., Orek C., Parlak A., Sarac K., Turkez H. and Tozlu Ö. Ö., "Synthesis, structure, cytotoxic and antioxidant properties of 6-ethoxy-4-methylcoumarin", *Journal of Molecular Structure*, 2020, 1205: 127577.
- [21] Zając A., Dymińska L., Lorenc J., Ptak M. and Hanuza J., "Syntheses, spectroscopic properties and molecular structure of silver phytate complexes-IR, UV-VIS studies and DFT calculations", *Journal of Molecular Structure*, 2018, 1156: 483-491.
- [22] Ramesh G. and Reddy B. V., "Spectroscopic investigation on structure (monomer and dimer), molecular characteristics and comparative study on vibrational analysis of picolinic and isonicotinic acids using experimental and theoretical (DFT & IVP) methods", *Journal of Molecular Structure*, 2018, 1160: 271-292.
- [23] Orief M. and Abdel-Rhman M., "Molecular modeling, spectroscopic and structural studies on newly synthesized ligand N-benzoyl-2-isonicotinoylhydrazine-1-carboxamide", *Journal of Molecular Structure*, 2018, 1173: 332-340.
- [24] OMER L. A. and ANWER R. O., "Population Analysis and UV-Vis spectra of Dopamine Molecule Using Gaussian 09", *Journal of Physical Chemistry and Functional Materials*, 2020, 3(2): 48-58.
- [25] Schlegel H. B., "Optimization of equilibrium geometries and transition structures", *Journal of Computational Chemistry*, 1982, 3(2): 214-218.
- [26] Frisch M., Trucks G., Schlegel H. B., Scuseria G. E., Robb M. A., Cheeseman J. R., Scalmani G., Barone V., Mennucci B. and Petersson G., "gaussian 09, Revision d. 01, Gaussian", Inc., Wallingford CT, 2009, 201.

- [27] KOPARIR P., Rebaz O., KARATEPE M. and AHMED L., "Synthesis, Characterization, and Theoretical Inhibitor Study for (1E, 1'E)-2, 2'-thiobis (1-(3-mesityl-3-methylcyclobutyl) ethan-1-one) Dioxime", *El-Cezeri*, 8(3): 1495-1510.
- [28] Sworakowski J., "How accurate are energies of HOMO and LUMO levels in small-molecule organic semiconductors determined from cyclic voltammetry or optical spectroscopy?", *Synthetic Metals*, 2018, 235: 125-130.
- [29] Adiguzel R., Aktan E., Evren E. and Çetin A., "A Computational Study on Some Pyridine-Substituted-Bis-1, 2, 4-Triazole Derivatives and Investigation of Their Catalytic Activities", *International Journal of Pure and Applied Sciences*, 2020, 6(2): 200-207.
- [30] Lu Y., Feng L., Jiang X., Zhao Y., Zhao G. and Yuan C., "Construction of a molecular structure model of mild-oxidized Chinese lignite using Gaussian09 based on data from FTIR, solid state ¹³C-NMR", *Journal of molecular modeling*, 2018, 24(6): 135.
- [31] Singh J., "IR and Raman spectra with Gaussian-09 molecular analysis of some other parameters and vibrational spectra of 5-fluoro-uracil", *Research on Chemical Intermediates*, 2020: 1-23.
- [32] Fun H.-K., Goh J. H., Wu D. and Zhang Y., "6-Methoxy-4-methyl-2H-chromen-2-one", *Acta Crystallographica Section E: Structure Reports Online*, 2011, 67(1): o136-o136.
- [33] Yavari I., Djahaniani H. and Nasiri F., "The crystal structure of tert-butyl coumarin-3-carboxylate", *Journal of the Iranian Chemical Society*, 2006, 3(1): 46-50.
- [34] Galvez E., Iriepa I., Lorente A., Mohedano J. M., Florencio F. and Garcia-Blanco S., "Synthesis and structural study of amins derived from 8-aminoquinoline and 1-aminonaphthalene", *Canadian journal of chemistry*, 1987, 65(4): 687-692.
- [35] Allen F. H., Kennard O., Watson D. G., Brammer L., Orpen A. G. and Taylor R., "Tables of bond lengths determined by X-ray and neutron diffraction. Part 1. Bond lengths in organic compounds", *Journal of the Chemical Society, Perkin Transactions 2*, 1987, (12): S1-S19.
- [36] Michl J., "Organic chemical systems, theory", *Catalysis, Homogeneous*, 1992: 474.
- [37] Wang J., Wang W., Wang X., Wu Y., Zhang Q., Yan C., Ma W., You W. and Zhan X., "Enhancing performance of nonfullerene acceptors via side-chain conjugation strategy", *Advanced Materials*, 2017, 29(35): 1702125.
- [38] AHMED L. and Rebaz O., "1H-Pyrrole, Furan, and Thiophene Molecule Corrosion Inhibitor Behaviors", *Journal of Physical Chemistry and Functional Materials*, 4(2): 1-4.
- [39] Amalanathan M., Rastogi V., Joe I. H., Palafox M. and Tomar R., "Density functional theory calculations and vibrational spectral analysis of 3, 5-(dinitrobenzoic acid)", *Spectrochimica Acta Part A: Molecular and Biomolecular Spectroscopy*, 2011, 78(5): 1437-1444.
- [40] Koparir M., Orek C., Alayunt N., Parlak A. E., Koparir P., Sarac K., Dastan S. D. and Cankaya N., "Synthesis, Structure Investigation, Spectral Characteristics and Biological Activities of 4-Benzyl-3-(2-Hydroxyphenyl)-1H-1, 2, 4-Triazole-5 (4H)-Thione", *Communications in Computational Chemistry*, 2013, 1: 244-268.
- [41] Pearson R. G., "Absolute electronegativity and hardness: applications to organic chemistry", *The Journal of Organic Chemistry*, 1989, 54(6): 1423-1430.
- [42] Omer R. A., Ahmed L. O., Koparir M. and Koparir P., "Theoretical analysis of the reactivity of chloroquine and hydroxychloroquine", *Indian Journal of Chemistry-Section A (IJCA)*, 2020, 59(12): 1828-1834.
- [43] Pearson R. G., "Absolute electronegativity and hardness correlated with molecular orbital theory", *Proceedings of the National Academy of Sciences*, 1986, 83(22): 8440-8441.
- [44] OMER R. A., Koparir P., Ahmed L. and Koparir M., "Computational and spectroscopy study of melatonin", *Indian Journal of Chemistry-Section B (IJC-B)*, 2021, 60(5): 732-741.
- [45] AHMED L. and Rebaz O., "Spectroscopic properties of Vitamin C: A theoretical work", *Cumhuriyet Science Journal*, 2020, 41(4): 916-928.
- [46] Rebaz O., KOPARIR P., QADER I. N. and AHMED L., "Structure reactivity analysis for Phenylalanine and Tyrosine", *Cumhuriyet Science Journal*, 2021, 42(3): 576-585.
- [47] Atkins P. and De Paula J., *Elements of physical chemistry*. 2009.
- [48] Palafox M. A., Bhat D., Goyal Y., Ahmad S., Joe I. H. and Rastogi V., "FT-IR and FT-Raman spectra, MEP and HOMO-LUMO of 2, 5-dichlorobenzonitrile: DFT study", *Spectrochimica Acta Part A: Molecular and Biomolecular Spectroscopy*, 2015, 136: 464-472.
- [49] Rebaz O., KOPARIR P., QADER I. and AHMED L., "Theoretical Determination of Corrosion Inhibitor Activities of Naphthalene and Tetralin", *Gazi University Journal of Science*: 1-1.
- [50] Koparir P., Sarac K. and Omar R. A., "Synthesis, molecular characterization, biological and computational studies of new molecule contain 1, 2, 4-triazole, and Coumarin bearing 6, 8-dimethyl", *Biointerface Research in Applied Chemistry*, 2022, 12(1): 809-823.
- [51] Jeyavijayan S. and Arivazhagan M., "Vibrational spectral investigation, NBO, first hyperpolarizability and UV-Vis spectral analysis of 3, 5-dichlorobenzonitrile and m-bromobenzonitrile by ab initio and density functional theory methods", *Spectrochimica Acta Part A: Molecular and Biomolecular Spectroscopy*, 2015, 136: 234-246.

- [52] KOPARIR P., Rebaz O., KARATEPE M. and AHMED L., "Synthesis, Characterization, and theoretical inhibitor study for (1E, 1'E)-2, 2'-thiobis (1-(3-mesityl-3-methylcyclobutyl) ethan-1-one) dioxime", *El-Cezeri*, 2020, 8(3): 1495-1510.
- [53] Omer R. A., Koparir P. and Ahmed L. O., "Characterization and Inhibitor Activity of Two Newly Synthesized Thiazole", *Journal of Bio-and Tribo-Corrosion*, 2022, 8(1): 1-12.